

Surface acoustic wave guiding in a diffractionless high aspect ratio transducer

Ludovic Socié, Sarah Benchabane, Laurent Robert, Abdelkrim Khelif, and Vincent Laude

Citation: *Appl. Phys. Lett.* **102**, 113508 (2013); doi: 10.1063/1.4795939

View online: <http://dx.doi.org/10.1063/1.4795939>

View Table of Contents: <http://apl.aip.org/resource/1/APPLAB/v102/i11>

Published by the [American Institute of Physics](http://www.aip.org).

Related Articles

Manipulation of the electron transport through a mesoscopic island by surface acoustic wave
J. Appl. Phys. **113**, 043717 (2013)

Ultrahigh-frequency surface acoustic wave generation for acoustic charge transport in silicon
Appl. Phys. Lett. **102**, 013112 (2013)

Surface acoustic wave nebulization on nanocrystalline ZnO film
Appl. Phys. Lett. **101**, 194101 (2012)

Manipulating particle trajectories with phase-control in surface acoustic wave microfluidics
Biomicrofluidics **5**, 044107 (2011)

Low-loss unidirectional transducer for high frequency surface acoustic wave devices
J. Appl. Phys. **110**, 076103 (2011)

Additional information on *Appl. Phys. Lett.*

Journal Homepage: <http://apl.aip.org/>


Journal Information: http://apl.aip.org/about/about_the_journal

Top downloads: http://apl.aip.org/features/most_downloaded

Information for Authors: <http://apl.aip.org/authors>

ADVERTISEMENT

JANIS Does your research require low temperatures? Contact Janis today.
Our engineers will assist you in choosing the best system for your application.



10 mK to 800 K
Cryocoolers
Dilution Refrigerator Systems
Micro-manipulated Probe Stations

LHe/LN₂ Cryostats
Magnet Systems

sales@janis.com www.janis.com
Click to view our product web page.

Surface acoustic wave guiding in a diffractionless high aspect ratio transducer

Ludovic Socié, Sarah Benchabane, Laurent Robert, Abdelkrim Khelif, and Vincent Laude
 Institut FEMTO-ST, Université de Franche-Comté, CNRS, ENSMM, UTBM, 32 avenue de l'Observatoire,
 F-25044 Besançon, France

(Received 1 February 2013; accepted 6 March 2013; published online 20 March 2013)

We demonstrate efficient three-dimensional surface acoustic wave guidance and confinement in a high-aspect ratio electrode transducer. Each electrode acts as an elastic resonator that is evanescently coupled to its neighbors. We observe high amplitude displacement fields confined within the high aspect ratio electrodes. The stored surface waves are found to present a general shear polarization instead of the sagittal polarization expected for classical Rayleigh waves. The elastic energy is mostly distributed in the mass-loaded areas, and waves propagate within the transducer without diffraction, even for very low acoustic apertures. © 2013 American Institute of Physics. [<http://dx.doi.org/10.1063/1.4795939>]

Surface acoustic wave (SAW) propagation can be easily perturbed by any structuration or alteration of the surface of a semi-infinite medium. This specificity, linked to the strong confinement of the elastic energy at the air/solid interface, has been widely exploited in view of ensuring SAW propagation control. Creation of locally slow or fast acoustic regions by surface doping or mass-loading has, for example, been used as a means of SAW waveguiding.¹⁻⁴ But a much tighter control of the surface-guided wave propagation properties can be achieved by surface structuration. It has, for instance, been shown that a periodic corrugation of the surface of isotropic^{5,6} substrates could induce shear horizontal (SH) waves that cannot be excited on a homogeneous surface, where only Rayleigh waves with sagittal polarization can be supported. The observation was extended to substrates with general anisotropy,^{7,8} hence demonstrating the potential brought by surface structuration for the control of the polarization properties of surface-guided waves. These corrugated surfaces can, besides, be seen as a one-dimensional equivalent of phononic crystals that are often considered as standing amongst the most promising ways to govern elastic wave propagation.⁹ They can also be compared with interdigital transducers (IDTs) that usually consist in a one-dimensional, periodical array of thin interleaved metal electrodes used for electrical transduction in a piezoelectric material. The combination of the two concepts, IDTs and strong corrugation, has been exploited to demonstrate the possibility to generate multimode, slow surface acoustic waves in high aspect ratio transducers (HAR).^{10,11} It has, in particular, been shown that the high aspect ratio electrodes actually act as resonators able to trap the elastic energy, therefore slowing down the wave velocity.¹² This capability to locally store the elastic energy inside a specifically designed structure and the mismatched polarizations that the wave generated by these HAR transducers exhibit compared to a flat, homogeneous substrate offer interesting prospect for the realization of highly efficient and compact SAW resonators. In this paper, we propose to bring this concept of HAR transducer a step further: inspired by recent works on phononic crystals of pillars deposited on a surface,^{13,14} we propose to limit laterally the dimension of the high aspect

ratio electrodes. To this aim, thin IDT electrodes are used as a basis for the proposed HAR device to ensure electrical conduction and piezoelectric signal generation. High aspect ratio structures are subsequently integrated and limited to the acoustic aperture of the initial transducer. This allows exciting self-standing, mechanically isolated resonators on a surface, hence laterally confining the mass-loading effect. Three-dimensional confinement of the elastic energy can, therefore, be obtained, and diffractionless SAW generation and waveguiding can be achieved in transducers with acoustic aperture widths as low as a one wavelength.

A scanning electron microscope image of a sample HAR IDT is shown in Figure 1. The transducers were fabricated on a lithium niobate substrate in the X-crystallographic orientation. Wave propagation is along the Y-axis, hence leading to an expected electro-mechanical coefficient k^2 of about 3.1%. First, an array of thin interleaved copper electrodes, linked by two busbars, is patterned on the substrate surface. This initial thin film acts as both a seed layer for the subsequent electroplating step and as a conductive layer for excitation of the HAR IDT. A thick photoresist

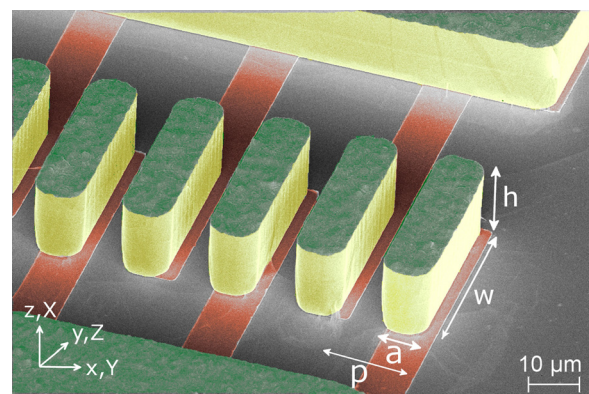


FIG. 1. Scanning electron microscope image of a W1 HAR IDT ($w/2p = 1$) with $h/2p = 0.43$ and $p = 18 \mu\text{m}$ (false colors). The copper seed layer used for electroplating and electrical conduction of the signal is shown in red, while the electroplated nickel appears in green. The plating was limited to the acoustical aperture length and to the IDT busbars. The reference frame (x, y, z) and crystallographic axes (X, Y, Z) are depicted as an inset.

(Microchemicals AZ9260) is then coated and patterned by UV lithography to shape a negative mould of the final thick metal resonators. These latter are grown by electroplating from a nickel sulfamate bath. The finger width a was set to $9\ \mu\text{m}$ for a transducer pitch $p = 2a = 18\ \mu\text{m}$, and the number of finger pairs was set either to 10 or 50. Because of the non-uniform distribution of the current flow on the surface during the electroplating process, a strong dispersion of the resonator height is observed from IDT to IDT, depending on their position on the wafer. The resonator height then ranges from 13 to $22.4\ \mu\text{m}$. This results in a distribution of the normalized $h/2p$ parameter that ranges from 0.36 to 0.62. In the case illustrated in Figure 1, the IDT has a normalized acoustic aperture $w/2p$ equal to one and, hence, an aperture width of $36\ \mu\text{m}$.

The HAR IDTs were characterized electrically by radio-frequency probe testing. Figure 2 displays the reflection scattering parameter measurements (S_{11}) obtained for two sets of HAR IDTs with normalized acoustic apertures, respectively, equal to $w/2p = 1$ (subsequently referred to as sample W1) and to $w/2p = 2$ (sample W2) for two different electrode heights in each case. Sample W1 is a 50 finger pair transducer while sample W2 has ten finger pairs, which mostly accounts for the resonance amplitude difference observed between the two transducers. Four resonances are identified for sample W1 versus five for sample W2. Each resonance corresponds to a propagating surface mode with phase velocity $v = 2f \times p$ but very low group velocity.¹² The resonance frequency depends on the electrode height and decreases when the $h/2p$ ratio increases, which agrees well with former theoretical and experimental results reported.^{10,11} The slowest surface mode reported here has a phase velocity of $1015\ \text{m/s}$, but velocities as low as $781\ \text{m/s}$ were measured on a W1 sample with $h/2p = 0.58$. The wave velocities are therefore significantly lower than the one expected for a classical Rayleigh wave that is around $3940\ \text{m/s}$. Most of the resonances remain beneath the sound line, which is set by

the velocity of the slowest bulk waves and that lies here at $109.4\ \text{MHz}$. The shaded area in Fig. 2 hence represents the radiative region of the substrate inside which the surface waves can be considered as leaky. The elastic energy carried by these different modes is then expected to be trapped by the electroplated structures. It can be noted, however, that the Q-factor of the resonances decreases with increasing resonance frequencies. This may be due to an increasing coupling of the generated surface-guided waves to surface waves of the surrounding substrate as their resonance frequency draws closer to the sound line.

The electrical measurements clearly show that well-defined resonances can be obtained from transducers exhibiting very low acoustic apertures, as low as $w = 2p$. This is a dramatic difference compared to the behavior expected from a low acoustic aperture thin IDT and indicates a very good confinement of the elastic energy inside the resonators that allows building up an efficient electro-acoustic response. But the waveguiding and energy storing capabilities of the fabricated HAR IDTs can be even more convincingly assessed by a mapping of the elastic energy at the substrate surface. To this aim, we performed an optical detection of the distribution of the elastic energy by laser scanning heterodyne interferometry. This well-known method has been successfully used for the characterization of various electro-acoustic devices¹⁵ although it only provides information on the out-of-plane component of the displacement field, meaning that it is blind to pure SH waves. One W1 and one W2 devices were investigated using this technique. Each of the elastic resonances numbered from A to I in Fig. 2 were probed. The optical scans were performed over an area of $120 \times 300\ \mu\text{m}^2$ and of $130 \times 350\ \mu\text{m}^2$, respectively, covering the entire length of the HAR IDTs. The scan step was set at $2\ \mu\text{m}$ in both directions. The measured data are then averaged along the transducer length to give a cross-section of the elastic energy distribution across the transducer aperture. The results are reported in Figs. 3 and 4.

A first striking observation is that all the elastic modes have a non-zero out-of-plane component, meaning that they exhibit a general shear polarization. This is a significant difference with the one-dimensional HAR IDTs, where the vertical and shear polarizations could be decoupled and therefore where generation of pure shear waves could be observed.¹¹ But the most interesting feature is the very strong confinement of the elastic energy, in particular, for the low frequency modes. Fig. 3 displays the measured out-of-plane mechanical displacement for the W1, $h/2p = 0.43$, 50-finger-paired HAR IDT. In the case of modes A and B, the acoustic field is confined in the electroplated areas. More precisely, the energy is located in the electrodes and propagation within the structure seems to occur as a result of evanescent coupling from one resonator to another. The maximum amplitude of displacement is reached at the edges of the resonating structures and can be in excess of $10\ \text{nm}$ for mode B ($f_r = 54.8\ \text{MHz}$, Fig. 3(b)), which is comparatively larger with respect to the nm-range displacement amplitude expected from a standard, thin IDT. The energy then abruptly decreases outside the resonators. The elastic wave is therefore guided along the transducer length, without diffraction or energy leakage outside the transducer acoustic

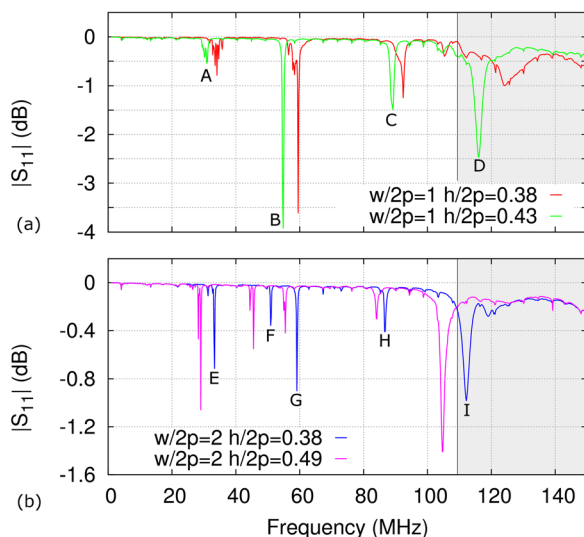


FIG. 2. (a) Measured electrical reflection $|S_{11}|$ as a function of frequency for two 50-finger-paired W1 HAR IDTs with $h/2p = 0.38$ and $h/2p = 0.43$. (b) $|S_{11}|$ parameter measurements for two W2 HAR IDTs with $h/2p = 0.38$ and $h/2p = 0.49$ and 10 finger pairs. The vertical line at $109.4\ \text{MHz}$ sets the position of the sound line that delimits the radiative area, here shaded in gray.

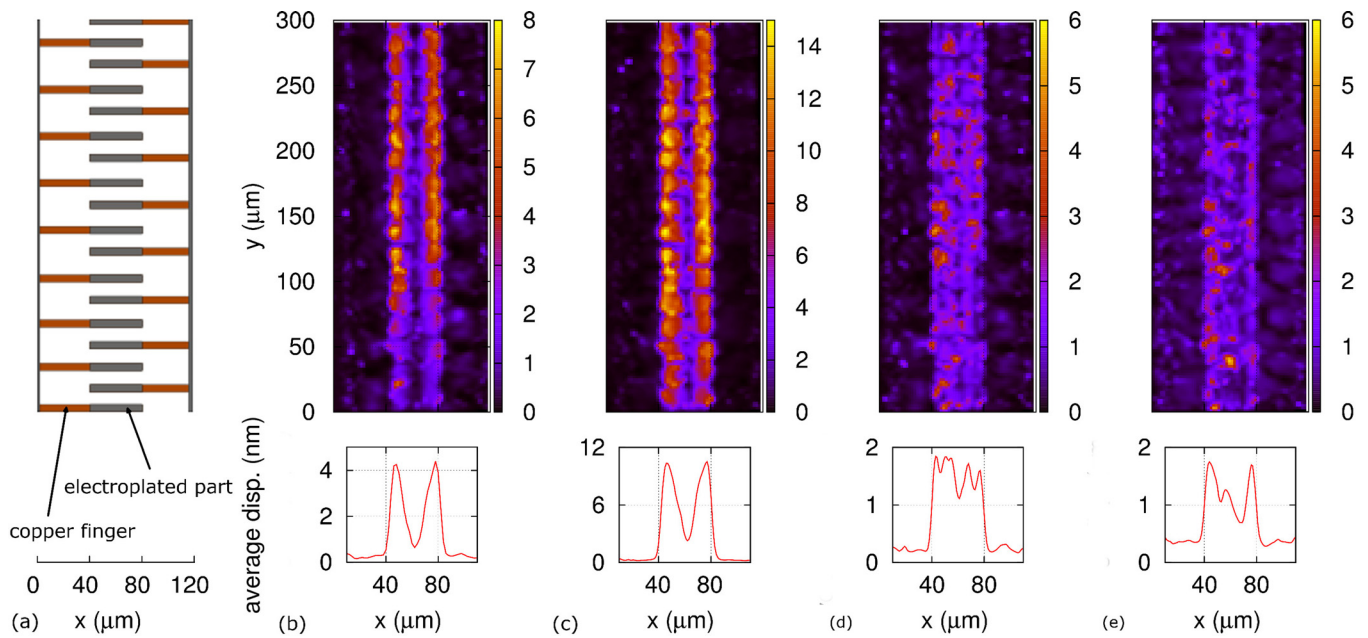


FIG. 3. Out-of-plane mechanical displacement and the average displacement along HAR IDT for each mode of a W1 HAR IDT ($w/2p=1$) with $h/2p=0.43\ \mu\text{m}$ and 50 fingers pairs. (a) Schematic of area scanned with optical probe, (b) mode A: $f=30.9\ \text{MHz}$, (c) mode B: $f=54.8\ \text{MHz}$, (d) mode C: $f=89.2\ \text{MHz}$, (e) mode D: $f=116.1\ \text{MHz}$.

aperture. As the resonant frequency increases, for instance, for modes C and D, the out-of-plane displacement amplitude decreases, and energy leakage to the surrounding homogeneous flat surface is clearly observed. A transverse modal structure also appears, much similarly to what can be observed in a classical waveguide with increasing width.

Very similar observations can be made from the optical characterization of the W2, $h/2p=0.38$, 10-finger-paired HAR IDT that are reported in Fig. 4. The maximum displacement amplitude is also reached for the second mode, vibrating at $f_r=52.6\ \text{MHz}$, and a decrease in amplitude with increasing frequencies is also noticed. Again, as clearly illustrated by modes G, H, and I, the number of transverse modes increases with frequency. In addition, a fifth mode appears

which agrees well with the waveguide picture for this HAR IDT structure: the number of guided modes increases as the waveguide width gets larger. The diffractionless property of the propagation is once again made obvious by the field maps, as energy leakage in the transverse direction is negligible. Figs. 4(a) and 4(b) show in addition that no propagation occurs outside the HAR IDT along the propagation direction either: the elastic energy is confined within the transducer and cannot be launched into the surrounding homogeneous surface. The mismatch between the modal shape of the VP/SH polarized modes of the resonators and the sagittally polarized waves of a homogeneous surface, combined with the significant difference in velocities, strongly hinders coupling from the HAR IDTs to the surrounding flat surface.

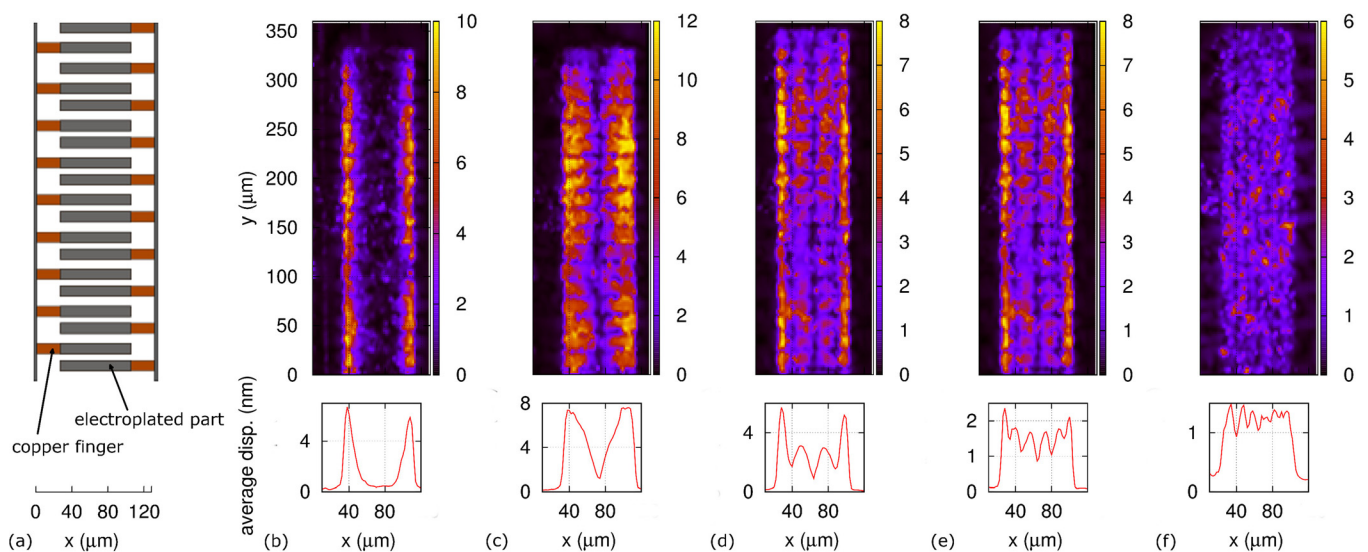


FIG. 4. Out-of-plane mechanical displacement and the average displacement along HAR IDT for each mode of a W2 HAR IDT ($w/2p=2$) with $h/2p=0.38\ \mu\text{m}$ and 10 fingers pairs. (a) Schematic of area scanned with optical probe, (b) mode E: $f=35.6\ \text{MHz}$, (c) mode F: $f=52.6\ \text{MHz}$, (d) mode G: $f=60\ \text{MHz}$, (e) mode H: $f=86.4\ \text{MHz}$, (f) mode I: $f=111.1\ \text{MHz}$.

Numerical simulations of an infinitely long HAR IDT of the W1 type further support this analysis. The wave motions of the electrode over one unit cell and one wave period are reported for modes A, B, and C.¹⁶ They clearly illustrate the strong confinement of the elastic energy within the electrode and confirm the general shear character of the polarization. A description of the simulation conditions is available in supplementary material.¹⁶

In summary, we have demonstrated efficient three-dimensional surface acoustic wave guidance and confinement in a high-aspect ratio electrode transducer. Each electrode is proved to act as a resonator able to store the elastic energy, hence significantly slowing down the surface wave velocity. This results in high amplitude displacement fields located within the HAR electrodes. Energy storage goes along with a change in the polarization properties of the surface wave as they present a general shear polarization instead of the sagittal polarization expected for classical Rayleigh waves. The velocity and polarization mismatch between the eigenmodes of the HAR IDT and those supported by a homogeneous flat surface leads to a very low conversion rate towards waves propagating in the surrounding medium. The elastic energy is therefore mostly distributed in the mass-loaded areas and waves propagate within the transducer without diffraction, even for very low acoustic apertures. A FEM computation is found to be in excellent agreement with the experimental observations. The obtained results open interesting prospects for the realization of highly confining SAW waveguides by decreasing further the effective width of the waveguide and reaching subwavelength

features. The resulting strong confinement of the elastic energy makes these transducers an ideal playground for surface interactions that could find applications to integrated acousto-optics or sensing.

This work has been carried out within project ANR-09-NANO-004 (phoxcry) funded by ANR (P3N2009) and received a partial support of the French RENATECH network through FEMTO-ST technological facility.

¹R. V. Schmidt, *Appl. Phys. Lett.* **27**, 8 (1975).

²P. Hartemann, P. Cauvard, and D. Desbois, *Appl. Phys. Lett.* **32**, 266 (1978).

³V. Hinkov, *J. Appl. Phys.* **62**, 3573 (1987).

⁴O. Peverini, H. Herrmann, and R. Orta, *IEEE Trans. Ultrason. Ferroelectr. Freq. Control* **51**, 1298 (2004).

⁵B. A. Auld, J.-J. Gagnepain, and M. Tan, *Electron. Lett.* **12**, 650 (1976).

⁶N. E. Glass and A. A. Maradudin, *Electron. Lett.* **17**, 773 (1981).

⁷A. N. Darinskii, *J. Acoust. Soc. Am.* **107**, 2447 (2000).

⁸I. Malfanti, A. Taschin, P. Bartolini, and R. Torre, *Europhys. Lett.* **97**, 44010 (2012).

⁹M. S. Kushwaha, P. Halevi, L. Dobrzynski, and B. Djafari-Rouhani, *Phys. Rev. Lett.* **71**, 2022 (1993).

¹⁰V. Laude, A. Khelif, T. Pastureaud, and S. Ballandras, *J. Appl. Phys.* **90**, 2492 (2001).

¹¹V. Laude, L. Robert, W. Daniau, A. Khelif, and S. Ballandras, *Appl. Phys. Lett.* **89**, 083515 (2006).

¹²M. Dühning, V. Laude, and A. Khelif, *J. Appl. Phys.* **105**, 093504 (2009).

¹³A. Khelif, Y. Achaoui, S. Benchabane, V. Laude, and B. Aoubiza, *Phys. Rev. B* **81**, 214303 (2010).

¹⁴Y. Achaoui, A. Khelif, S. Benchabane, L. Robert, and V. Laude, *Phys. Rev. B* **83**, 104201 (2011).

¹⁵K. Kokkonen and M. Kaivola, *Appl. Phys. Lett.* **92**, 063502 (2008).

¹⁶See supplementary material at <http://dx.doi.org/10.1063/1.4795939> for full details on the numerical simulations and videos corresponding to modes A, B and C.